Bull. Mater. Sci. (2019) 42:93
https://doi.org/10.1007/s12034-019-1809-1

Fe/Fe_3O_4 nanocomposite powders with giant high magnetization values by high energy ball milling

V RAMYA, A GANGWAR, S K SHAW, N K MUKHOPADHYAY and N K PRASAD*
Department of Metallurgical Engineering, Indian Institute of Technology (Banaras Hindu University), Varanasi 221005, India
*Author for correspondence (nandkp.met@iitbhu.ac.in)

MS received 3 August 2018; accepted 19 November 2018; published online 27 March 2019

Abstract. The present work reports on the relatively higher saturation magnetization values of Fe/Fe_3O_4 nanocomposites. For example, the nanocomposites of Fe obtained after milling for 10 h with 5, 10 and 15 wt% of Fe_3O_4 had displayed saturation magnetization values of 210, 238 and 216 $Am^2\,kg^{-1}$, respectively, in contrast to 218 $Am^2\,kg^{-1}$ of bulk Fe. Similarly, the maximum magnetization values for the nanocomposites after 20 and 30 h of milling were 215 and 190 $Am^2\,kg^{-1}$ for the sample containing 5 and 15 wt% of Fe_3O_4, respectively. The values of H_C and M_r suggest that nanocomposites exhibit soft ferromagnetic behaviour. The ball milling also reduced the crystallite and particle size of Fe from microndimension to nanometres. This was confirmed from X-ray diffraction, transmission electron microscopy and scanning electron microscopy analyses. The crystallite size of pure Fe decreased to 35, 20 and 19 nm, respectively, for the samples having 5, 10 and 15 wt% of Fe_3O_4 after 10 h of milling. The crystallite size decreased further with increased milling time.

Keywords. Nanocomposites; high energy ball mill; Fe_3O_4; magnetization.

1. Introduction

Nanocomposites are the class of materials which exhibit high performance, due to their unusual property combinations and design possibilities [1]. They have at least one phase with nanoscale dimensions (0-D, 1-D, 2-D and 3-D) and can be reinforced either in a metal, ceramic or polymer matrix. These nanoscale second phases create a synergy between various constituents and could enhance their properties to meet the required expectations [1]. Materials exhibiting magnetic properties (e.g., ferromagnetic, ferrimagnetic and antiferromagnetic) can be utilized as a matrix and reinforcement to obtain nanocomposites with enhanced magnetic properties [2,3]. In these systems, the magnetic exchange interaction is altered due to the exchange coupling interaction between the constituents. This type of exchange coupled magnetic material is suitable for applications, in particular permanent magnets [4], magnetic recording media [5] or magnetic hyperthermia [6]. The properties of such materials are dependent on the shape, size and distribution of the reinforced particles [7].

There are many routes to produce metal matrix nanocomposites such as the liquid state process, solid state process, vapour deposition, semi-solid state process and *in-situ* fabrication technique [8–11]. Out of these, the non-equilibrium processing technique like mechanical attrition (or milling) has been utilized successfully to obtain such nanocomposites as well as nanocrystalline metals and alloys [12–17]. In this process, materials undergo continuous fracturing and their size reduces to nanodimension. However, due to the associated welding phenomenon, their overall particle size enhances to microdimension though the crystallite size remains in nanodimension [12]. In the initial stages of milling, both the ductile (metals/alloys) and brittle (ceramics or intermetallics) components display different responses. The former gets flattened by the collisions whereas the latter one gets fragmented [12–17]. During milling, the fragmented particles get trapped in between ductile particles. As milling proceeds, due to work hardening of the ductile phase, the spacing between them reduces and the brittle phase gets distributed uniformly. This happens for the brittle materials which are insoluble in the ductile matrix. For the soluble phase, they utilize alloys thereby maintaining chemical homogeneity [12–17]. Thus, fine ceramic dispersed alloys (e.g. ODS) can also be produced easily by this method otherwise, it is extremely difficult *via* conventional melting because of the differences in their density [18–20]. There are number of reports on the preparation of ceramic/metal nanocomposites, such as Fe/Fe_3O_4, Fe/Al_2O_3, Fe/ZnO, Cu/Fe_3O_4 and Fe/ZrO_2 using mechanical milling [13–17,20–22]. These materials have received significant consideration due to their attractive mechanical, electrical and magnetic properties. For example, Fe/Fe_3O_4 composites were synthesized by Ding *et al*. [14] using ball milling of an equimolar mixture of the two powders. The authors have observed high coercivity (H_C) values for the as-prepared composites due to the

increased defects during ball milling. Nevertheless, the H_C values reduced upon annealing because of strain relievement upon heat treatment. Few researchers have also reported on the production of nano-crystalline magnetite (Fe_3O_4) by milling of hematite (Fe_2O_3) with iron (Fe) in a stoichiometric proportion [23].

To the best of our knowledge, there are hardly any reports where nanoparticles of ceramics in general and magnetite (Fe_3O_4) in particular are used to obtain nanocomposite powders with Fe. The nanoparticles were used with the expectation that these will restrict the welding phenomenon during milling of Fe and hence will give nanopowders. Thus, in the present work, we used Fe_3O_4 nanoparticles (∼5–20 nm) as reinforcement which was synthesized by a microwave refluxing technique. It was ball milled with varying compositions of Fe (∼53 μm) up to 30 h of duration. The samples were analysed using X-ray diffraction (XRD), transmission electron microscopy (TEM), scanning electron microscopy (SEM) and magnetic property measurement system (MPMS).

2. Experimental

Fe_3O_4 nanoparticles with a particle size of ∼5–20 nm were collected from our laboratory [24]. These superparamagnetic Fe_3O_4 nanoparticles were taken in varying concentrations of 5, 10 and 15 wt% and were added to Fe powders having an average particle size of 53 micron. These powders were milled using a Retsch PM400 high energy ball mill. The ball to powder ratio was taken as 10:1 and the milling speed was kept at 200 rpm. The balls and vials used were of tungsten carbide. Toluene was used as a process controlling agent. The samples were collected after each 10, 20 and 30 h of milling. The nomenclature for the sample identification with various compositions of Fe_3O_4, which were collected after different durations of milling, are listed in table 1.

The powder samples obtained after various milling times were subjected to characterization techniques such as XRD, TEM, SEM and MPMS. The XRD patterns for all the powder samples were recorded using an X-ray powder diffractometer (Rigaku Miniflex 600) with CuKα radiation ($\lambda = 1.54056$ Å) from 20 to 80° with a step of 10° min^{-1}. The crystallite size of the samples was estimated from the broadening of peaks using Scherrer's equation [25]:

$$t = 0.9\lambda/\beta \cos\theta$$

where β is the full width at half maximum in radians after considering the instrumental correction, θ is the diffracted angle in degrees and λ is the wavelength of the radiation and the lattice strain was evaluated using

$$\beta_{\text{strain}} = 4\varepsilon \tan\theta$$

where ε is the strain in the material.

Table 1. Nomenclature of the samples obtained after various milling time periods.

%wt Concentration of Fe_3O_4	Milling time (h)	Nomenclature
0	10	F0F1
	20	F0F2
	30	F0F3
5	10	F5F1
	20	F5F2
	30	F5F3
10	10	F10F1
	20	F10F2
	30	F10F3
15	10	F15F1
	20	F15F2
	30	F15F3

The morphology and size of the nanocomposite powders were estimated by TEM (FEI Technai G^2). For this purpose, few milligrams around 0.1 mg of powder were dispersed in methanol (∼15 ml) and then sonicated for 15 min. Two drops of homogenized solution was then placed on a carbon-coated copper grid and allowed it to get dried prior to observation under TEM. The selected area electron diffraction (SAED) patterns were also taken under standard conditions for these samples. For SEM analysis (FE-SEM, Carl Zeiss, Supra-40), a small amount of the powder sample (∼10 mg) was dispersed in methanol (∼15 ml) solution and it was sonicated for 15 min. The dried powder was placed on the carbon tape which was then placed over the sample holder and then subjected to the analysis. The magnetic measurements (hysteresis loops) for the samples were carried out using a SQUID based magnetometer (MPMS®3, Quantum design) at room temperature and in an external magnetic field up to ±2 T.

3. Results and discussion

The XRD patterns of the Fe samples obtained after different durations of milling are shown in figure 1. There are no significant changes in the positions of the peaks of Fe even after milling for 30 h but these have broadened (figure 1a–c). Similarly, Fe–5% Fe_3O_4 milled samples did not show any considerable change in the XRD patterns and these could be indexed as pure Fe phase (figure 1d–f). There were no peaks for Fe_3O_4 as its concentration was lower than the detection limit of the X-ray diffractometer. Nevertheless, an increase in the width of the peaks was observed with increased milling time. The peak widths for these samples were more than those for pure Fe samples under similar conditions (figure 1).

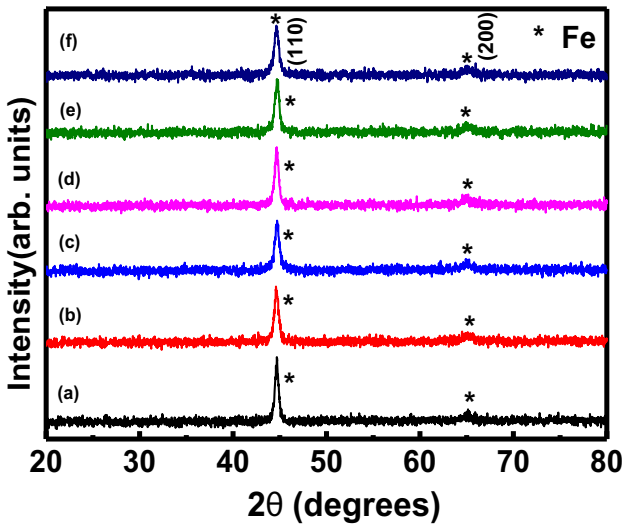

Figure 1. XRD patterns of (**a**) F0F1, (**b**) F0F2, (**c**) F0F3, (**d**) F5F1, (**e**) F5F2 and (**f**) F5F3.

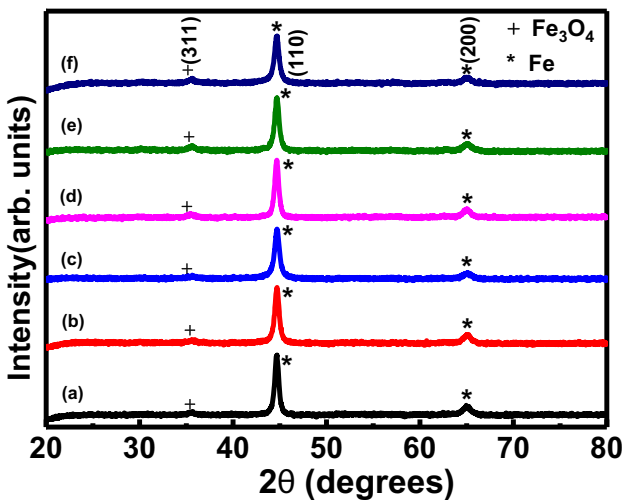

Figure 2. XRD patterns of (**a**) F10F1, (**b**) F10F2, (**c**) F10F3, (**d**) F15F1, (**e**) F15F2 and (**f**) F15F3.

The XRD patterns of the composites with 10 and 15 wt% of Fe_3O_4 and after milling for 10, 20 and 30 h are shown in figure 2. Few peaks of Fe_3O_4 were observed for these samples (figure 2). The width of the peaks was found to be increasing with increased milling time as similar to that of previous samples. The samples with higher contents of Fe_3O_4 had relatively wider peaks and were thus expected to have a much smaller crystallite and particle size.

Similar to earlier observations, the crystallite size of the samples was found to be decreasing with increased milling duration [11–17] (figure 3). This could be attributed to the fracture–welding–fracture phenomena of ductile materials which generally occur during milling [11–17]. The

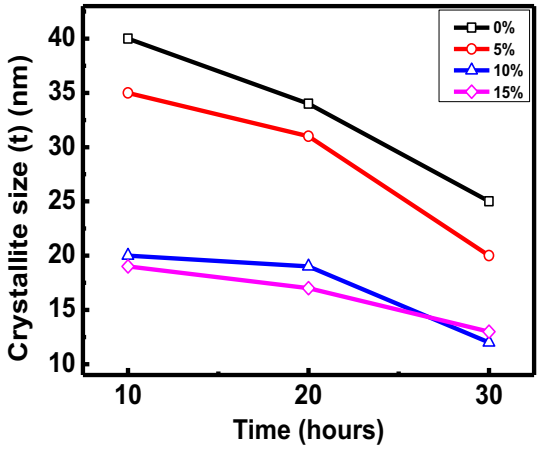

Figure 3. Variation of crystallite size with composition and time of milling.

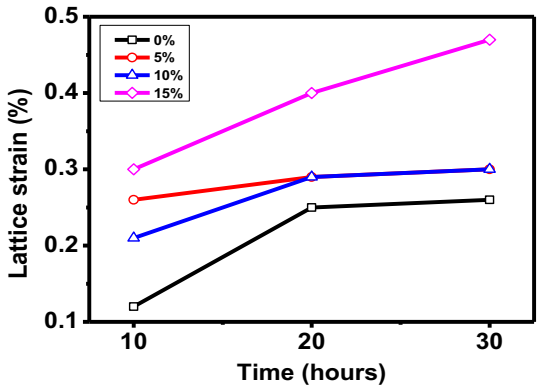

Figure 4. Variation of lattice strain with composition and time of milling.

crystallite size of pure Fe decreased from 53 μm to 40, 34 and 25 nm after 10, 20 and 30 h of milling, respectively (figure 3). For the composites with 5 wt% of Fe_3O_4, the crystallite size decreased to 35, 31 and 20 nm after 10, 20 and 30 h of milling, respectively (figure 3). Relatively larger size reduction in the crystallite size for these samples could be accomplished due to the presence of ceramic phase Fe_3O_4 (particle size ~5–20 nm). This oxide phase might have restricted the welding phenomenon that occurred during ball milling for ductile materials. The strength and hardness of nanosized oxides are generally higher than those of their bulk counterpart and hence act as an abrasive help in reducing their size. Similarly, the crystallite size of the other two composites F10F3 and F15F3 also reduced with milling time and it was 12 and 13 nm after 30 h of milling (figure 3).

The variation in the lattice strain with increased time of milling is observed in figure 4. The lattice strain is observed to generally enhance with increased milling time for all the samples with a few exceptions. It has been reported that during

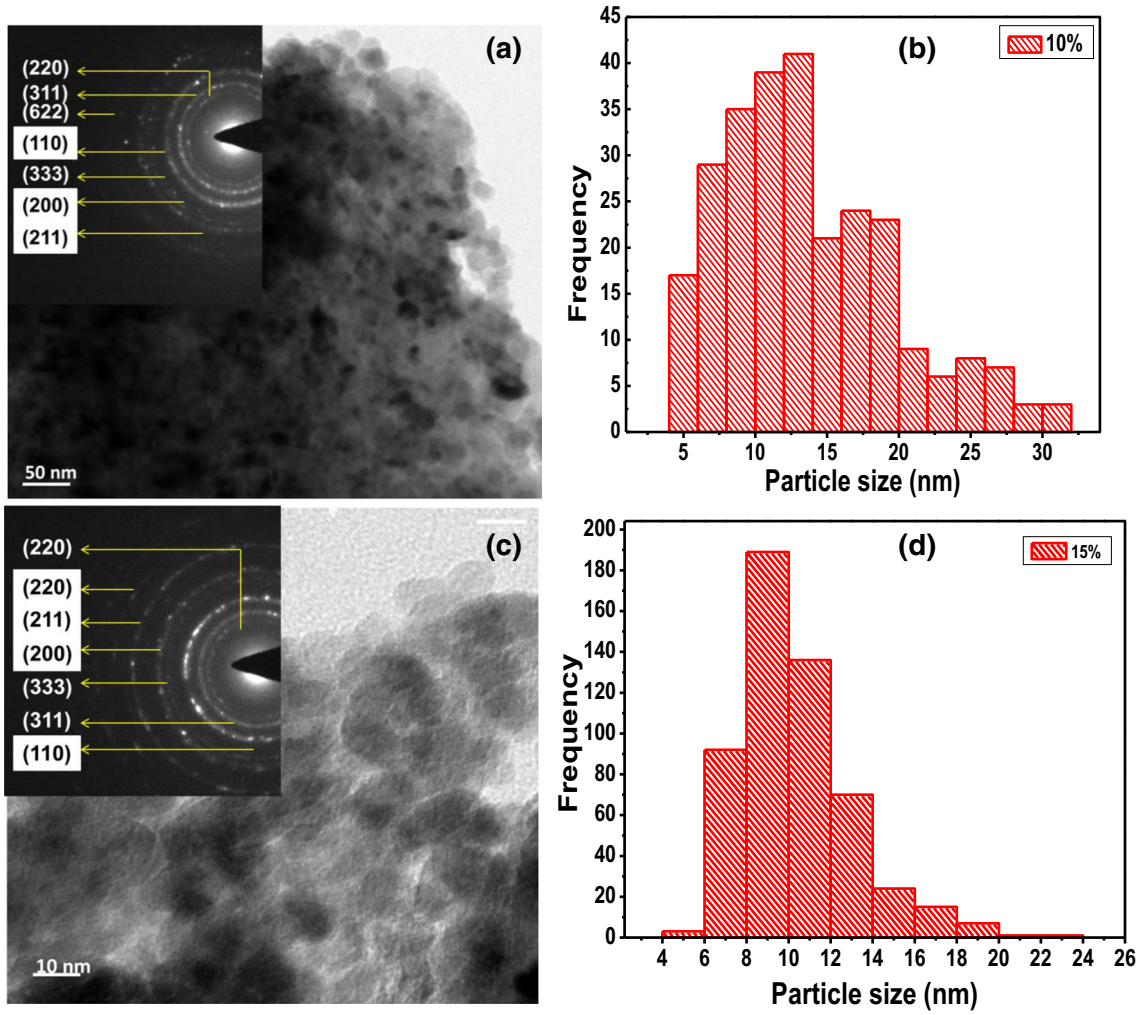

Figure 5. (**a**) TEM micrographs of F10F3, (**b**) corresponding particle size distribution, (**c**) TEM micrographs of F15F3 and (**d**) corresponding particle size distribution. The insets of figures show the corresponding SAED patterns. The planes with a white background represent the BCC phase and the others indicate the FCC phase.

mechanical alloying, heavy deformations are introduced into the particles which induce a variety of crystal defects such as dislocations, vacancies, stacking faults, and increased number of grain boundaries which generate strains in the lattice [12].

The typical TEM micrographs of F10F3 obtained after 30 h of milling are shown in figure 5a. The micrograph suggests that some of the particles had a spherical morphology and these were agglomerated. The size of the particles ranges between 5 and 30 nm and their average size was 15 ± 2 nm. The distribution of the size for this sample is shown in figure 5b. The size below the crystallite size of Fe represents nanoparticles of Fe_3O_4. In the present case, the welding of Fe was restricted by the ceramic phase Fe_3O_4 nanoparticles. Furthermore, the oxide phase also acts as a nanoabrasive that helps in the reduction of the particle size of Fe into nanodimension. The inset of figure 5a affirms the presence of both Fe and Fe_3O_4 in the particles. Similarly, figure 5c displays the micrograph of the F15F3 sample obtained after 30 h of milling which indicates the spherical nature of some of the particles. The particles seem to be agglomerated. The inset of figure 5c confirms the XRD findings that Fe and Fe_3O_4 coexist in the sample. The size distribution of this sample is shown in figure 5d which further affirms that the size of the particles ranges between 5–25 nm and the average particle size was 10 ± 2 nm. However, it should be noted here that these were the supernatant particles used for TEM analysis.

For further investigation, the microstructures of F0F1, F0F3, F5F1, F5F3, F10F3 and F15F3 were collected from SEM and compared (figure 6). For F0F1 samples, the microstructure has micron sized chips which are basically of pure iron (figure 6a) and are similar to that of the ductile particles obtained after ball milling [26]. The shape of the particles is an indication of fracture–welding–fracture phenomena that occur during milling. In contrast to this, figure 6b shows the microstructure of F5F1 where finer particles are also visible along with the coarser ones. The smaller particles obtained

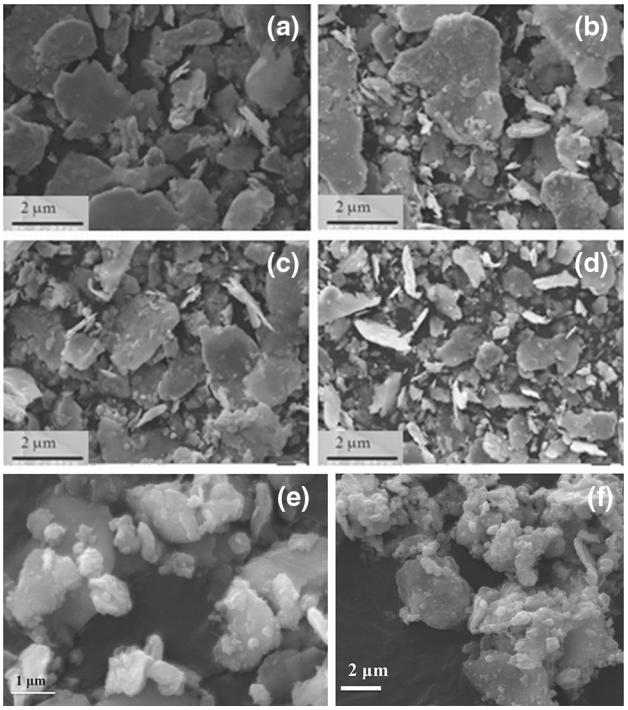

Figure 6. SEM micrographs of (**a**) F0F1, (**b**) F5F1, (**c**) F0F3, (**d**) F5F3, (**e**) F10F3 and (**f**) F15F3 samples.

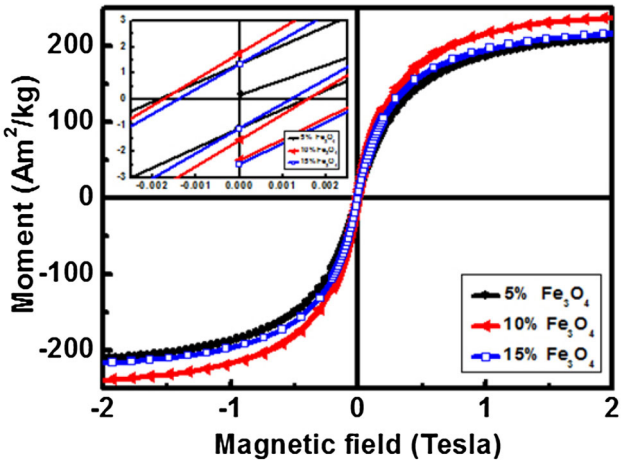

Figure 7. Magnetization *vs*. field curves at room temperature and up to ±2 T for samples milled for 10 h.

in this case could be due to the presence of Fe_3O_4 nanoparticles which might have reduced the welding of the particles during milling. This was further confirmed from figure 6d for F5F3 which had significantly large amounts of smaller particles as compared to that of F0F3 (figure 6c). Similarly, as the concentration of oxide nanoparticles increased in the samples (F10F3 and F15F3) the particle size was found to be decreasing (figure 6e and f). For these two samples, the micron sized particles seem to be composed of agglomerated nanoparticles and were similar to that of milled Fe_3O_4 samples observed by Marinca *et al* [27]. The samples under TEM seem like nanoparticles as the agglomerated particles break during ultrasonication and the supernatant was used for the characterization (figure 5a). However, such nanoparticle formation using high energy ball milling has not been observed for metals and alloys [23–28].

The typical magnetization *vs*. field curves for the as-milled Fe/Fe_3O_4 nanocomposites obtained after 10 h of milling at 300 K and up to ±2 T of field are shown in figure 7. The M_S values were 210, 238 and 216 $Am^2\,kg^{-1}$ for F5F1, F10F1 and F15F1 samples, respectively. The M_S values obtained for the nanocomposites were even higher than that for bulk Fe (~218 $Am^2\,kg^{-1}$) [29]. The nanoparticles of Fe_3O_4 which was used as reinforcement had a M_S value around 60 $Am^2\,kg^{-1}$ [30]. Thus, as per the rule of mixture for composites, the effective M_S values should have diminished. But, the increase in the M_S values for nanocomposites suggests that some magnetic exchange interactions occurred at the boundaries of nanoparticles of Fe_3O_4 and Fe [31]. For an increased milling duration of 20 h, the M_S value for F5F2 increased but for other two F10F2 and F15F2, it got reduced. In contrast, the M_S values for F5F3 and F10F3 decreased but for Fe15F3, it improved after 30 h of milling as compared to that of previous milling duration (i.e. 20 h). The maximum M_S value was around 190 $Am^2\,kg^{-1}$ for the Fe15F3 sample. This was despite the fact that the sample had a significant amount of nanoparticles of Fe. The earlier reports suggest that Fe having nanosized particles can have M_S values in the range of 60–150 $Am^2\,kg^{-1}$ [32]. As discussed earlier, the obtained higher values of M_S for nanocomposites were due to the exchange coupling amongst the nanoparticles of two phases [31]. Nevertheless, the reduction in the M_S values could be due to the formation of a magnetic dead layer on the surface of the nanocomposites. Because of the two competitive phenomena, a general trend for variation in the M_S values was not observed.

The inset of figure 7 shows hysteresis loops, which suggest the presence of ferro- or ferrimagnetic particles. The variations in the H_C values with increased milling durations for all the three samples are shown in figure 8b. The H_C values were nearly 1.8, 1.7 and 1.3 mT for F5F1, F10F1 and F15F1 samples, respectively, which indicates that the samples had a soft magnetic behaviour. With increased milling time, the H_C values were found to be increasing for all the samples. This could be attributed to the particle size reduction and the introduction of defects during high energy ball milling. Further, the M_r values of the F5F1, F10F1 and F15F1 samples were around 1.3, 1.3 and 1.7 $Am^2\,kg^{-1}$, respectively. The values were similar to those of soft magnetic materials. Like H_C values, the M_r values were also found to be increasing and this may be attributed to the interactions between the magnetic components in the nanocomposites.

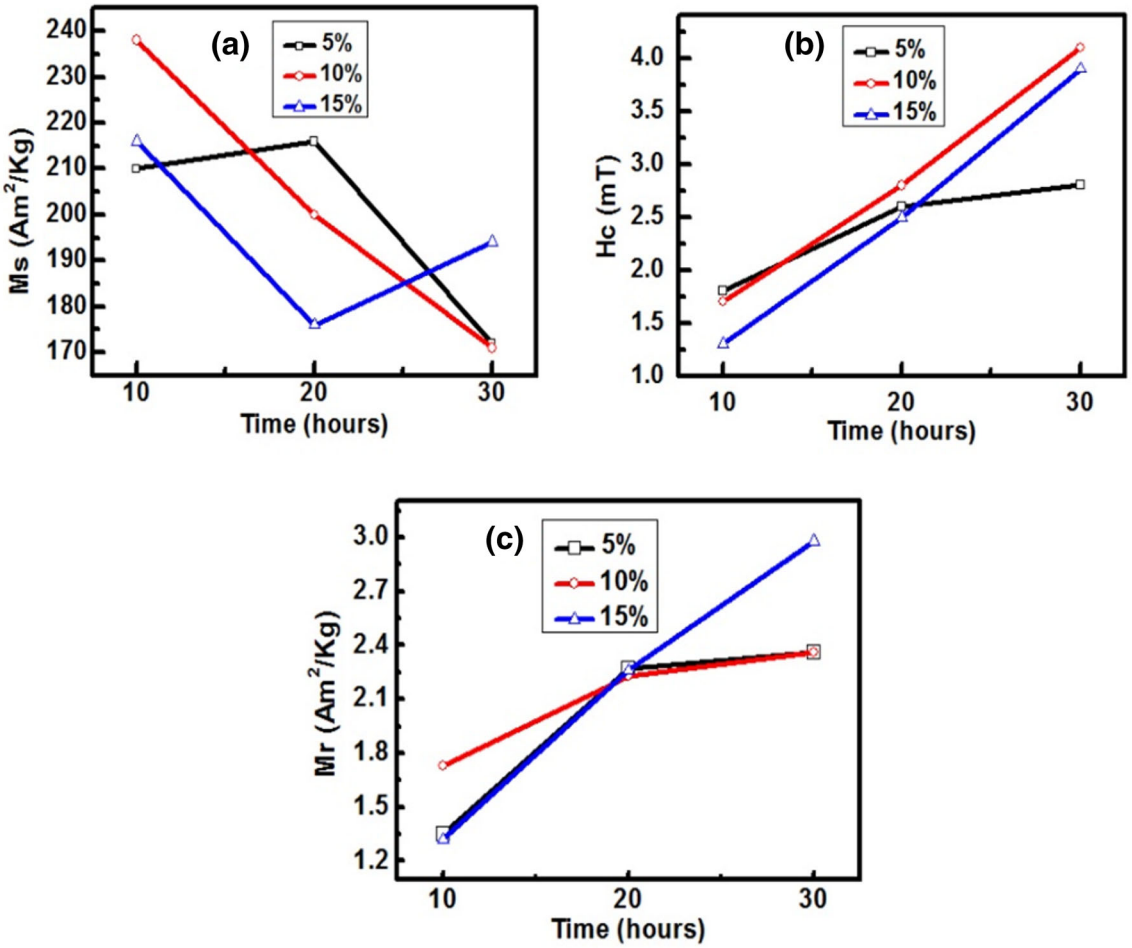

Figure 8. (**a**) Saturation magnetization (M_S), (**b**) coercivity (H_C) and (**c**) remnant magnetization (M_R) of samples with respect to milling time.

4. Conclusions

The high energy ball milling process has helped to obtain nanocomposite powders of Fe/Fe_3O_4 with varying compositions. The oxide phase acted as a nanoabrasive and reduced the particle size of Fe from micron to nanodimension. The XRD and TEM results confirmed the coexistence of the two phases having their size in the nanometric range. The highest M_S value of 238 $Am^2\ kg^{-1}$ has been achieved for Fe with 10% Fe_3O_4 after 10 h of milling. This value was higher than that of bulk Fe but too high as compared to that of nanoparticles of Fe or Fe_3O_4. Nanocomposites with such a high M_S value may be very useful for several applications.

References

[1] Camargo P H C, Satyanarayana K G and Wypych F 2009 *Mater. Res.* **12** 1
[2] Rowe M P 2015 *US Patent and Trademark Office U.S. Patent* No. 9,093,205B2 (Washington, DC)
[3] Prischepa S L, Danilyuk A L, Prudnikava A L, Komissarov I V, Labunov V A, Yanushkevich K I 2014 in: *Nanomagnetism* J M Gonzalez Estevez (ed) (Manchester, UK: One Central Press) 227
[4] Skomski R and Coey J M D 1993 *Phys. Rev. B* **48** 15812
[5] Kapoor M and Victora R H 2007 *IEEE Trans. Mag.* **43** 2289
[6] Lee J H, Jang J T, Choi J S, Moon S H, Noh S H, Kim J W *et al* 2011 *Nature Nanotech.* **6** 418
[7] Spaldin N A 2010 *Magnetic materials: fundamentals and applications* (Cambridge: Cambridge University Press)
[8] Rosso M 2006 *J. Mater. Process. Technol.* **175** 364
[9] Singh H, Sarabjit N J and Tyagi A K 2011 *J. Engg. Res. Stud.* **2** 72
[10] Ceschini L, Dahle A, Gupta M, Jarfors A E W, Jayalakshmi S, Morri A *et al* 2017 *Aluminum and magnesium metal matrix nanocomposites* (Singapore: Springer)
[11] Casati R and Vedani M 2014 *Metals* **4** 65
[12] Suryanarayana C 2008 *Rev. Adv. Mater. Sci.* **18** 203
[13] Bonetti E, Del Bianco L, Signoretti S and Tiberto P 2001 *J. Appl. Phys.* **89** 1806
[14] Zhao L, Yang H, Li S, Yu L, Cui Y, Zhao X *et al* 2006 *J. Magn. Magn. Mater.* **301** 287
[15] Ding J, Miao W F, Street R and McCormick P G 1996 *Scripta. Mater.* **35** 1307

[16] Linderoth S R and Pedersen M S 1994 *J. Appl. Phys.* **75** 5867
[17] Kosmac T and Courtney T H 1992 *J. Mater. Res.* **7** 1519
[18] Pardavi H M and Takacs L 1993 *J. Appl. Phys.* **73** 6958
[19] Zhang L, Ukai S, Hoshino T, Hayashi S and Qu X 2009 *Act. Mat.* **57** 3671
[20] Suryanarayana C, Klassen T and Ivanov E 2011 *J. Mater. Sci.* **46** 6301
[21] Jha P, Gupta P, Kumar D and Parkash O 2014 *J. Compos. Mater.* **48** 207
[22] Raghavendra K G, Das Gupta A, Bhaskar P, Jayasankar K, Athreya C N, Panda P *et al* 2016 *Powder Technol.* **287** 190
[23] Reis M A L, Rodrigues E M S, Nero J D, Simões S, Viana F, Vieira M F *et al* 2015 *Mater. Sci. Engg. B* **5** 311
[24] Petrovský E, Alcala M D, Criado J M, Grygar T, Kapička A and Šubrt J 2000 *J. Magn. Magn. Mater.* **210** 257
[25] Gangwar A, Alla S K, Srivastava M, Meena S S, Prasadrao E V, Mandal R K *et al* 2016 *J. Magn. Magn. Mater.* **401** 559
[26] Tiwary C S, Kashyap S, Biswas K and Chattopadhyay K 2013 *J. Phys. D: Appl. Phys.* **46** 385001
[27] Marinca T F, Chicinaş H F, Neamţu B V, Chicinaş I, Isnard O, Popa F *et al* 2016 *Adv. Powder Technol.* **27** 1588
[28] Pelegrini L, Bittencourt S D, Pauletti P, Verney J C K D, Dias M D M and Schaeffer L 2015 *Mater. Res.* **18** 1070
[29] Crangle J and Goodman G M 1971 *Proc. R Soc. Lond. Ser. A, Math. Phys. Sci.* **321** 477
[30] Woo K, Hong J, Choi S, Lee H W, Ahn J P, Kim C S *et al* 2004 *Chem. Mater.* **16** 2814
[31] Yoon T J, Lee H, Shao H and Weissleder R 2011 *Angew. Chem. Int. Ed.* **50** 4663
[32] Chiriac H, Moga A E and Gherasim C 2008 *J. Optoelectron. Adv. Mat.* **10** 3492